

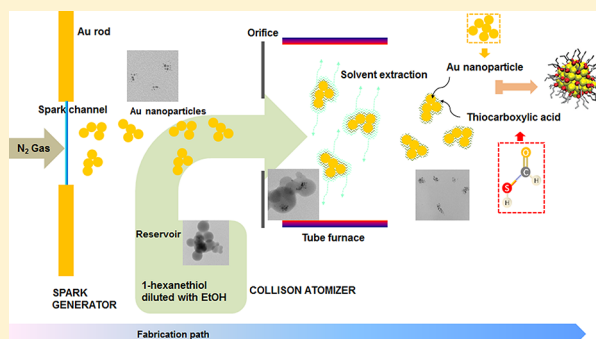
Aerosol Based Fabrication of Thiol-Capped Gold Nanoparticles and Their Application for Gene Transfection

Jeong Hoon Byeon[†] and Jeffrey T. Roberts^{*,†}[†]Department of Chemistry, Purdue University, West Lafayette, Indiana 47907, United States

S Supporting Information

ABSTRACT: In this study, an ambient-spark-produced-Au-nanoparticle-laden nitrogen gas was mixed with an atomized solution of 1-hexanethiol [$\text{CH}_3(\text{CH}_2)_5\text{SH}$] and ethanol (EtOH). The Au nanoparticles reacted with 1-hexanethiol in the atomized droplets to form capped gold nanoparticles, whose size distributions were measured for varying volumetric fractions of 1-hexanethiol. By increasing the thiol concentration from 0.1% to 1.0% (v/v), the size distribution of merged particles (Au–thiol) was changed from bimodal (showing a superposition of individual distributions of Au and droplets) to unimodal (showing only a droplet-like distribution, with the Au distribution eliminated) configuration. The latter phenomenon is attributed to quantitative incorporation of Au nanoparticles into atomized particles. Measurements of cell viability and transfection revealed that even though the merged particles had a higher cytotoxicity ($\sim 78\%$ in cell viability $> \sim 49\%$ for polyethyleneimine, PEI) than that did chitosan ($\sim 96\%$), the transfection (2.56×10^6 in RLU mg^{-1}) of gene was higher than those for chitosan (7.63×10^4) and PEI (6.84×10^5).

KEYWORDS: aerosol fabrication, thiol-capped, Au nanoparticle, gene transfection



■ INTRODUCTION

The Au nanoparticle system is one of the most extensively studied nanoparticle systems and is built upon the well understood interaction of organic functional groups with Au surfaces.¹ Functionalized Au nanoparticles have been considered to be very promising components of nanoelectronic devices,² and key elements of materials for biomedical applications, due to their compatibility with these systems.³ Thiol-capped gold (Au–SR) nanoparticles can be used as sensitive probes of gas and vapor concentration,⁴ as magnetic materials in data storage devices,⁵ for selective drug delivery,⁶ and for biomedical imaging.⁷ Because of the strong interaction between sulfur and gold, gold nanoparticles capped by thiol self-assembled layers are easily synthesized and are known to exhibit remarkable stability and ease of functionalization compared to other metal systems.^{5a,d,8} The presence of a thiol capping layer has been shown to influence the kinetics of growth and to confer advantages for size-controlled and disperse nanoparticle syntheses.⁹

The usual route to functionalized gold nanoparticles is wet chemistry. In contrast to classical wet chemical methods, aerosol processing involves a much more limited number of preparation steps.⁹ It also produces materials continuously, allowing for a straightforward collection of particles and generating low waste. The combination of aerosol processing and more conventional chemical routes has the potential to bring a “wind of change” to the synthesis of advanced nanomaterials.¹⁰ In this work, functionalized gold nanoparticles

were synthesized “on the fly” in a serial aerosol reactor (Scheme 1). Spark generated Au nanoparticles¹² (3 L min^{-1} , N_2 gas) passed over a collision atomizer (1.00% (v/v) 1-hexanethiol solution, EtOH based) orifice (0.3 mm diameter) where they mixed with atomized particles to form hybrid droplets. The droplets then passed through a heated tubular flow reactor operating at a 90°C wall temperature to drive ethanol from the droplets, resulting in thiol-capped nanoparticle gold. This low-temperature based serial aerosol reactor was recently described and applied to the fabrication of biocompatible inorganic–organic nanocomposites.¹³ Conventional aerosol-based flame reactor synthesis of functionalized Au nanoparticles typically requires high temperatures ($>2,000 \text{ K}$) and can only be used to fabricate or deposit inorganic nanoparticles.¹⁴ Such high temperatures can induce decomposition of organic components (i.e., biocompatible nanomaterials). For this reason, the aerosol equivalent of a one-pot approach is not a viable strategy for synthesizing biocompatible nanomaterials without expensive and time-consuming postfunctionalization steps.¹³

■ EXPERIMENTAL PROCEDURE

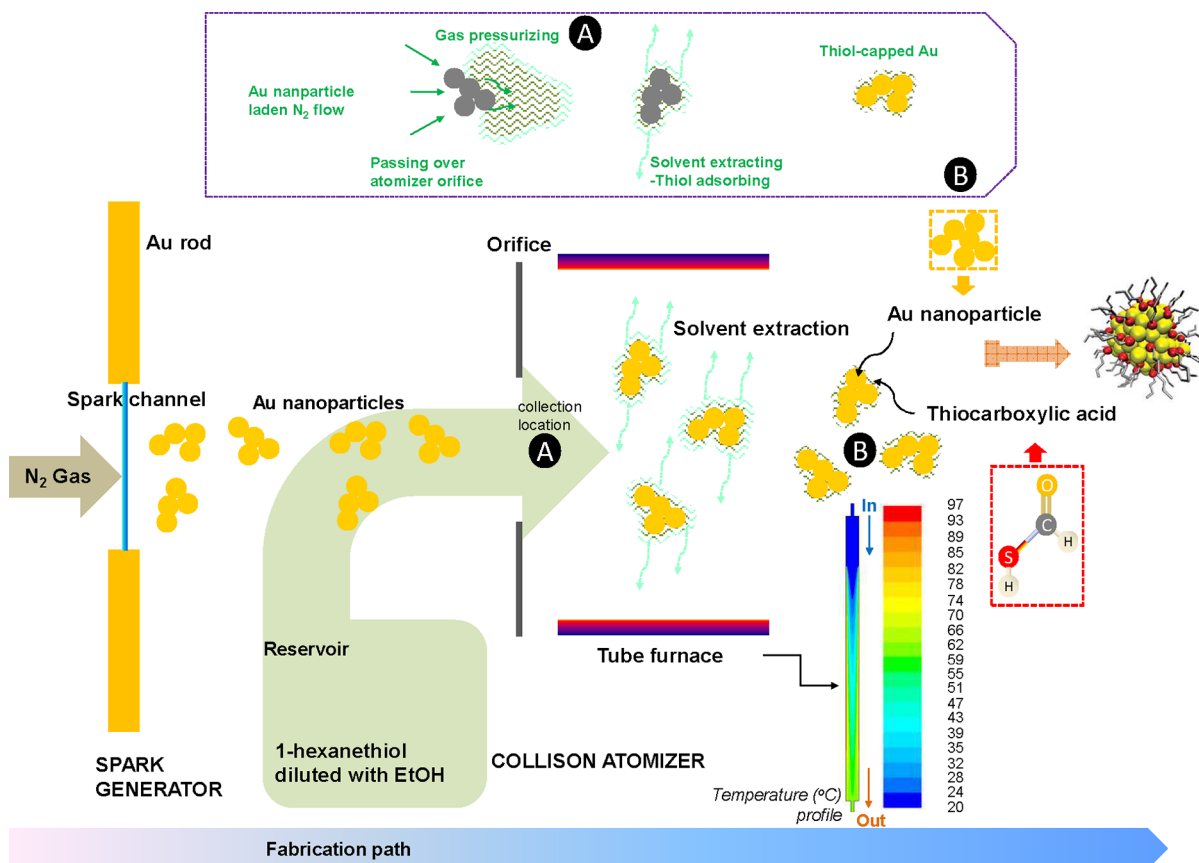
The size distributions of the aerosol particles are measured using a scanning mobility particle sizer (SMPS), consisting of an electrostatic classifier (3085, TSI, US), condensation particle counter (3776, TSI,

Received: February 23, 2012

Revised: June 8, 2012

Published: August 27, 2012

Scheme 1. Aerosol Based Fabrication of Thiol-Capped Au Nanoparticles



US), and an aerosol charge neutralizer (4530, HCT, Korea). The SMPS system, which measures the mobility equivalent diameter, is operated at a sample flow of 0.3 L min^{-1} , a sheath flow of 3.0 L min^{-1} , and a scan time of 135 s (measurement range: 4.61–156.8 nm). The SMPS measurements were performed after particles had exited the furnace region. TEM (CM-100, FEI/Philips, US) images were obtained at an accelerating voltage of 19–180 kV. Specimens were prepared for examination in the TEM by direct electrostatic aerosol sampling at a sampling flow of 0.3 L min^{-1} and an operating voltage of 5 kV using a Nano Particle Collector (NPC-10, HCT, Korea). For FTIR analysis (Figure 1), samples were prepared using polytetra-

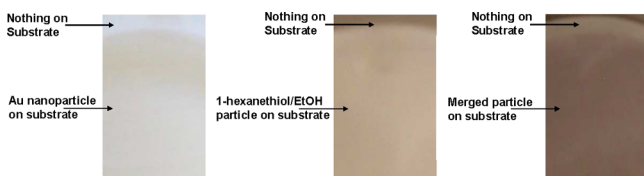


Figure 1. Photographs of sampled substrates for Au, 1-hexanethiol/EtOH, and merged particles.

fluoroethylene (PTFE) media substrate ($0.2 \mu\text{m}$ pore size, 47 mm diameter, 11807-47-N, Sartorius, Germany) by physical filtration (i.e., mechanical filtration mainly by diffusion, of particles on the surfaces of the substrate), and the spectra were recorded on a Nicolet 6700 FTIR spectrometer (Thermo Electron, US). The spectra were taken of samples in the range of $4000\text{--}400 \text{ cm}^{-1}$ in absorbance mode. The zeta potential of sample/pDNA complexes was determined using a zeta potential analyzer (Nano ZS-90, Malvern Instruments, UK). The samples were mixed with pDNA and incubated at room temperature for 30 min. The complexes were then diluted with double deionized water to an appropriate concentration. Measurements of the zeta

potential were carried out at 25°C and calculated using the manufacturer's supplied software.

Before *in vitro* measurements, the sampled particles on a PTFE substrate were detached in an ultrasound bath for 10 s. 1×10^6 HEK 293 cells preincubation in a 24-well culture plate for 24 h were replaced separately with the merged particle and control samples. After being challenged with the different samples, cells were replaced with 2 mL of culture medium containing MTT assay reagent (4 mg mL^{-1}) and incubated for additional 4 h. The resulting purple crystals were dissolved in 2 mL of dimethyl sulfoxide (DMSO). 250 μL of the DMSO solutions from the culture wells were loaded into a 96-well plate. Absorbances were measured at 570 nm by an ELISA plate reader (Thermo Multiskan Spectrum, US). The percentage cell viability was related to untreated control cells.

HEK 293 cells were seeded at a density of 1×10^5 cells well^{-1} in 24-well plate. The cells were treated with polyplex solution containing 2 mg of pDNA at various weight ratios for 4 h at 37°C . Luciferase activity was measured with a luminometer (TD-20/20, Promega, US). The final luciferase activity was expressed as RLU mg^{-1} of protein. An inverted fluorescent microscope (DMI 4000 B, Leica, Germany) was used to observe the EGFP expression of the polyplexes in the 293 cells.

■ RESULT AND DISCUSSION

Figure 2 summarizes results of the size distributions of Au, the atomized hexanethiol/EtOH solution, and the merged particles. The total number concentration (TNC), geometric mean diameter (GMD), and geometric standard deviation (GSD) of the merged particles are $2.35 \times 10^6 \text{ particles cm}^{-3}$, 25.3 nm, and 1.93, respectively, as shown in Figure 2a. The same data for pure Au nanoparticles are $6.50 \times 10^6 \text{ particles cm}^{-3}$, 19.4 nm, and 1.46, respectively, and for the atomized hexanethiol/EtOH droplets are $1.17 \times 10^6 \text{ particles cm}^{-3}$, 30.7 nm, and 1.71,

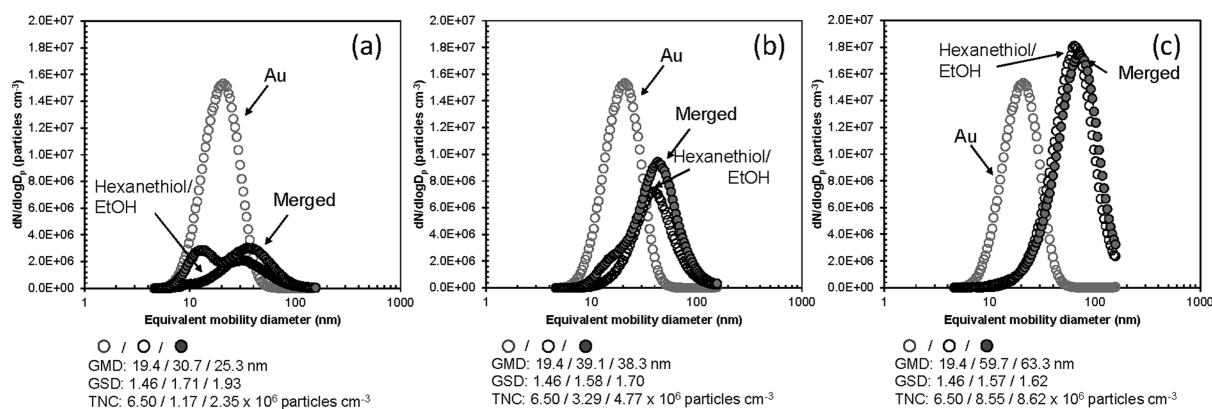


Figure 2. Size distributions of the spark generated Au, collision atomized hexanethiol/EtOH, and merged particles. The fabrication was applied using (a) 0.1% (v/v), (b) 0.5% (v/v), and (c) 1.0% (v/v) thiol concentrations (in EtOH). The spark generated Au, hexanethiol/EtOH, and merged particles are gray (unfilled), black (unfilled), and black (gray filled) circles, respectively.

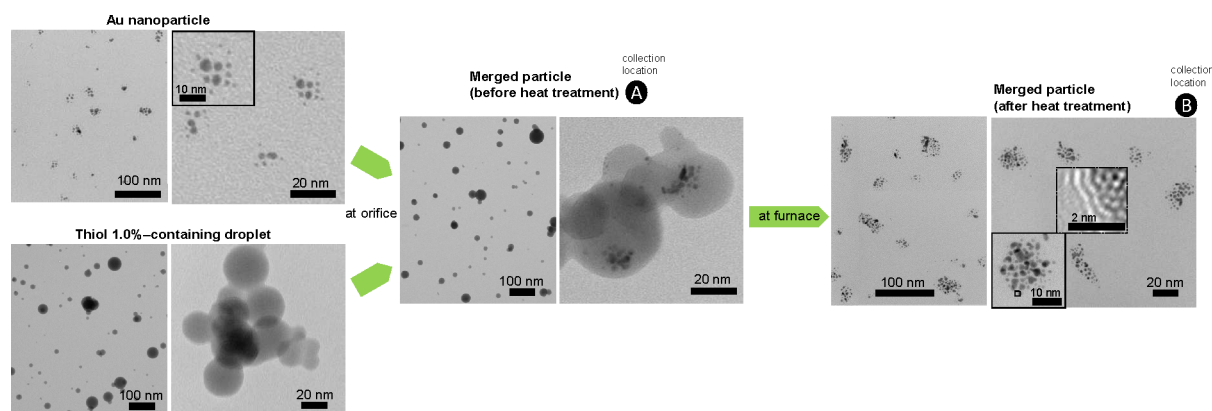


Figure 3. TEM images of spark generated Au and collision atomized hexanethiol/EtOH (left) and merged (center, before passing through the tube furnace; right, after passing through the tube furnace) particles.

respectively. For merged particles (at thiol 0.1%), although a large proportion of the Au nanoparticles were incorporated into larger hexanethiol/EtOH droplets, some of the Au nanoparticles remain in the initial state. This implies that the number concentration of hexanethiol/EtOH droplets was not sufficient to collect all the Au nanoparticles at the orifice outlet. The size distributions after the merging of the Au particles and atomized hexanethiol/EtOH droplets changed when the thiol concentration was increased to 1.0%, as shown in Figure 2b–2c. In Figure 2c, the Au nanoparticles are shown to be nearly quantitatively incorporated into atomized hexanethiol/EtOH droplets. The production rate of the merged particles for the 1.0% thiol solution was $6.7 \times 10^{-5} \text{ g min}^{-1}$. Scale-up would depend on the rate of spark nanoparticle Au generation. The development of high Au number output systems may enhance production rate for the functionalized particle fabrication. The size distribution of the merged particles (for the 1.0% solution) is similar to the atomized droplets. This implies that nearly quantitative incorporation of the Au nanoparticles into the hexanethiol/EtOH droplets may be possible at ~1.0% thiol concentration. The apparently enhanced incorporation higher hexanethiol/EtOH droplet concentration may originate from an increased collision frequency,¹⁵ dC/dt

$$\frac{dC_p}{dt} \propto \frac{2kTd_{pp}}{3\mu d_{bp}} C_{pp} C_{bp} \quad (1)$$

where C_{pp} and C_{bp} are the number concentrations of Au particles and hexanethiol/EtOH droplets, respectively; d_{pp} and d_{bp} are the respective diameters of Au particles and hexanethiol/EtOH droplets, respectively; kT is the Boltzmann factor; and μ is the gas viscosity.

In a previous study of a similar system, the sizes of ~60 nm metal nanoparticle agglomerates decreased when the particles passed over the atomizer. This was attributed to a shattering effect caused by rapid changes in pressure, density, and velocity across an orifice. For the present case, an analogous shattering phenomenon is not evident. This suggests that the shattering effect may be suppressed for smaller Au agglomerates, as implied by the following formula

$$D_p = \alpha \sqrt{\frac{D_{pa} H}{6\pi \Delta P \Theta^2}} \quad (2)$$

where D_p is the size of a restructured agglomerate, α is the proportionality constant, H is the Hamaker constant, ΔP is the pressure difference between the front and the rear of an orifice, and Θ is the parameter controlling the maximum cohesive strength between constituting particles in an agglomerate. From eq 2, the rate of shattering for 20 nm sized agglomerates is estimated to be about 3.4 times smaller than that of the 60 nm agglomerates studied previously.¹⁶ Therefore, a decrease in the size distribution for the merged particles from the droplet could not be observed. UV-vis spectra (Supporting Information)

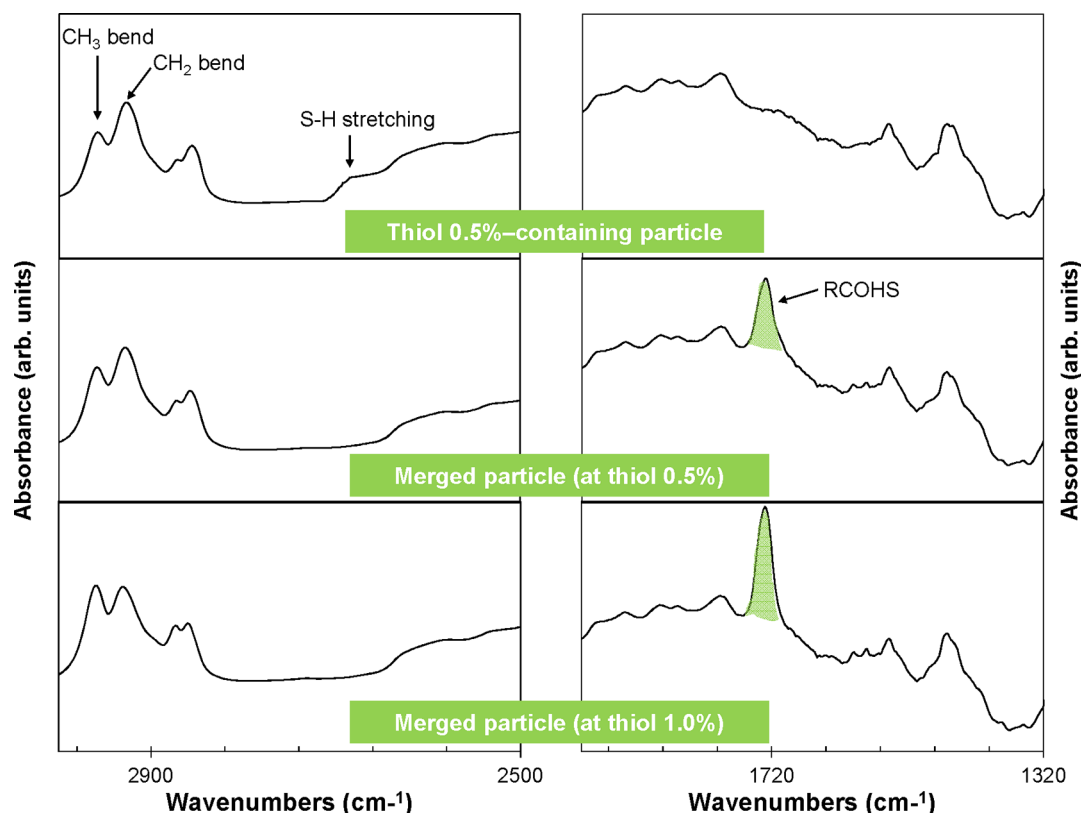


Figure 4. IR spectra of atomized 1-hexanethiol/EtOH and merged particles.

were consistent with the size distributions of the Au and merged (for the 1.0% solution) particles.

Figure 3 shows representative low and high magnification TEM images of collected Au particles, hexanethiol/EtOH droplets, and merged particles. Merged particles were collected both before and after passing through the tube furnace. The mean mode diameters of Au and the droplet particles are 16 ± 4.1 nm and 52 ± 11.2 nm, respectively. The center image shows that Au nanoparticles collected at the orifice outlet were entirely incorporated into atomized droplets. After thermal treatment in the tube reactor, the size of the embedded Au nanoparticles increased from ~ 16 to ~ 28 nm, whereas the overall sizes of the merged particles shrank due to evaporation of volatile material. The condition for complete evaporation can be estimated by considering the time required for the evaporation of the droplets and comparing it with the appropriate residence time in a tube furnace. The characteristic time to saturate gas with vapor from evaporating droplets, τ , is given *via* the equation

$$\tau = \frac{1}{2\pi D_d \delta_v C(D_d)} \quad (3)$$

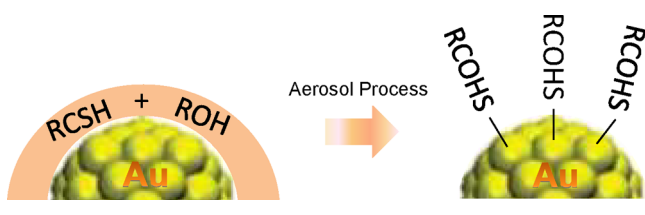
where D_d is the diameter of the droplet, δ_v is the diffusivity of the vapor, and $C(D_d)$ is the droplet number concentration. The estimated and applied residence times were 16.8 and 17.6 s, respectively, which implies that experimental conditions were sufficient to drive off all of the solvent completely. The increase of the Au nanoparticle size may have originated in part from coalescence between the incorporated Au nanoparticles in a droplet during heat treatment. The morphologies of the Au nanoparticles also changed. Specifically, the spherical shapes of primary particles evolved to more irregular shapes, and the

particle surfaces became more corrugated (see an inset of the right image in Figure 3). This may originate from the adsorption of thiol molecules, resulting in an interaction between S and Au.¹⁷ The morphologies of the merged particles is consistent with thiol-capped Au nanoparticles reported in previous reports.¹⁸ The production yield of thiol-capped Au nanoparticles is approximately 90%.

We attribute the shape change in gold to a chemical reaction with 1-hexanethiol (Scheme 1). The interaction between Au nanoparticles and 1-hexanethiol was investigated by FTIR spectroscopy. Figure 4 shows FTIR spectra of merged particles and of atomized hexanethiol/EtOH droplets. For the atomized droplet samples, the most prominent spectral features are at $\sim 2,920$ and $\sim 2,850$ cm^{-1} , corresponding to the symmetric and antisymmetric methylene stretching vibrations, respectively.¹⁹ These peaks were also presented in the spectra in merged particles. However, there is a pronounced difference between the merged particle and atomized droplet samples in the methylene stretching ($3,000$ – $2,800$ cm^{-1}) and S–H stretching ($\sim 2,700$ cm^{-1}) regions.²⁰ In fact, no S–H stretching band is observed for the merged particles, which we attribute to a reaction of S–H in 1-hexanethiol with the gold surface.^{19b} Also, a peak at $1,720$ cm^{-1} was clearly observed in the merged particles but not for the atomized droplets. The intensity of the $1,720$ cm^{-1} is more intense for particles that were synthesized with the more concentrated 1-hexanethiol solution. This suggests that the S–H bond reacts with the Au surface to form a product we assign as an adsorbed thiocarboxylate–Au (Scheme 2), formed by oxidative chemisorption.^{19c–e} Thiocarboxylate formation is anticipated on thiophilic metals such as Au.

We tested the cytotoxicity and gene transfection properties of merged particles as a potential material for biomedical

Scheme 2. Thiol-Capped Au Formation during Aerosol Processing



applications. Human embryonic kidney (HEK) 293 cells were incubated with merged particles (at thiol 1.0%) for 24 h, and cell viability was determined through a standard MTT [3-(4,5-dimethylthiazol-2-yl)-diphenyltetrazolium bromide] assay (Figure 5a). The particles were detached from the PTFE substrate by immersing the samples in water and subjecting them to ultrasound treatment for 10 s. The results show that cell viability was $\sim 78\%$ for the merged particles (cf. $\sim 86\%$ for the spark generated Au nanoparticles), while the measured viabilities of the PEI and chitosan control systems were $\sim 49\%$ and $\sim 96\%$, respectively. This implies that the merged particles have a biocompatibility that may be suitable in a clinical context. PEI and chitosan have been widely applied in biomedical applications because of their excellent properties such as biocompatibility, nontoxicity, or biodegradability.²¹ We next examined the ability of the merged particles to transfect HEK 293 cells using plasmid DNA (pDNA) that contain the luciferase and enhanced green fluorescent protein (EGFP) gene. The transfection efficiencies of sample/pDNA complexes in the HEK 293 cell line were higher than that of naked DNA (Figure 5b). The efficiency for the merged particles was the highest, even higher than those of chitosan and PEI. The inset of Figure 5b shows fluorescence of HEK 293 cells for the merged particles derived from EGFP expression, which further confirmed the transfection. The higher efficiency of the merged particles could relate to the zeta potentials (19.7 ± 4.85 : Au–thiol $> 13.3 \pm 1.91$: PEI $> -1.59 \pm 0.60$: chitosan) of sample/pDNA complexes and might also ascribe to the combination of high affinity between the luciferase and merged particles and relatively small size (~ 60 nm) of the merged particles (cf. ~ 120 nm for PEI and ~ 165 nm for chitosan, Supporting Information).

CONCLUSIONS

For the first time, an aerosol-based method has been used to construct thiol-capped Au nanoparticles. These results further establish aerosol processing as an efficient, scalable, and generalizable method for designing and fabricating an extraordinary broad range of functionalized nanobiomaterials.

ASSOCIATED CONTENT

Supporting Information

The UV–vis spectra of spark generated Au and thiol-capped Au nanoparticles and size distributions of aerosol PEI and chitosan particles. This material is available free of charge via the Internet at <http://pubs.acs.org>.

AUTHOR INFORMATION

Corresponding Author

*Phone: (+1-765) 494-1730. Fax: (+1-765) 494-1736. E-mail: jtrob@purdue.edu. Corresponding author address: Department of Chemistry, Purdue University, Mathematical Sciences Building, 150 N. University Street, West Lafayette, IN 47907-2067, USA.

Notes

The authors declare no competing financial interest.

ACKNOWLEDGMENTS

This work was partially supported by NSF grant CHE-0924431. We also thank H. -K. Kim for assistance in acquiring the results of *in vitro* definitions.

REFERENCES

- (1) (a) Landman, U.; Luedtke, W. D. *Faraday Discuss.* **2004**, *125*, 1. (b) Schreiber, F. *Prog. Surf. Sci.* **2000**, *65*, 151.
- (2) (a) Dong, X.; Huang, W.; Chen, P. *Nanoscale Res. Lett.* **2011**, *6*, 60. (b) Yajadda, M. M. A.; Levchenko, I.; Han, Z. J.; Ostrikov, K. *Appl. Phys. Lett.* **2010**, *97*, 163109. (c) Homberger, M.; Simon, U. *Philos. Trans. R. Soc. A* **2010**, *368*, 1405. (d) Chirea, M.; Pereira, C. M.; Silva, F. J. *Phys. Chem. C* **2007**, *111*, 9255.
- (3) (a) Kim, J.; Sadowsky, M. J.; Hur, H.-G. *Biomacromolecules* **2011**, *12*, 2518. (b) Qian, J.; Jiang, L.; Cai, F.; Wang, D.; He, S. *Biomaterials* **2011**, *32*, 1601. (c) Shiang, Y.-C.; Huang, C.-C.; Wang, T.-H.; Chien, C.-W.; Chang, H.-T. *Adv. Funct. Mater.* **2010**, *20*, 3175. (d) Wang, Z.; Zong, S.; Yang, J.; Song, C.; Li, J.; Cui, Y. *Biosens. Bioelectron.* **2010**, *26*, 241. (e) Kim, D.; Jeong, Y. Y.; Jon, S. *ACS Nano* **2010**, *4*, 3689.
- (4) (a) Hanwell, M. D.; Heriot, S. Y.; Richardson, T. H.; Cowlam, N.; Ross, I. M. *Colloids Surf., A* **2006**, *284–285*, 379. (b) Chow, E.; Gengenbach, T. R.; Wieczorek, L.; Raguse, B. *Sens. Actuators, B* **2010**, *143*, 704.
- (5) (a) Crespo, P.; Litrán, R.; Rojas, T. C.; de la Fuente, J. M.; Sánchez-López, J. C.; García, M. A.; Hernando, A.; Penadés, S.; Fernández, A. *Phys. Rev. Lett.* **2004**, *93*, 087204. (b) Crespo, P.; García, M. A.; Fernández-Pinel, E.; de la Venta, J.; Merino, J. M.; Quesada, A.; Hernando, A.; Fernández, A.; Penadés, S. *Acta Phys. Pol., A* **2008**, *113*, 515. (c) Crespo, P.; Guerrero, E.; Muñoz-Márquez, M. Á.; Hernando, A.; Fernández, A. *IEEE Trans. Magn.* **2008**, *44*, 2768. (d) Guerrero, E.; Muñoz-Márquez, M. Á.; García, M. A.; Crespo, P.; Fernández-Pinel, E.; Hernando, A.; Fernández, A. *Nanotechnology* **2008**, *19*, 175701.
- (6) Dreaden, E. C.; Mwakwari, S. C.; Sodji, Q. H.; Oyelere, A. K.; El-Sayed, M. A. *Bioconjugate Chem.* **2009**, *20*, 2247.

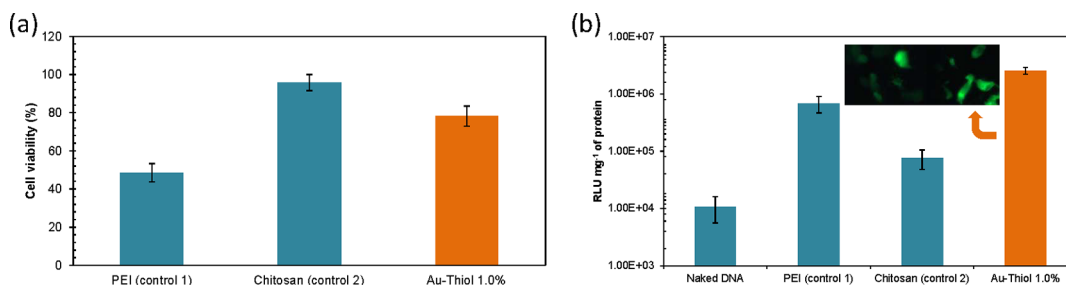


Figure 5. *In vitro* measurements of (a) cell viability and (b) gene transfection efficiency for merged particles.

- (7) Liu, C.-L.; Ho, M.-L.; Chen, Y.-C.; Hsieh, C.-C.; Lin, Y.-C.; Wang, Y.-H.; Yang, M.-J.; Duan, H.-S.; Chen, B.-S.; Lee, J.-F.; Hsiao, J.-K.; Chou, P. T. *J. Phys. Chem. C* **2009**, *113*, 21082.
- (8) (a) Zanchet, D.; Tolentino, H.; Alves, M. C. M.; Alves, O. L.; Ugarte, D. *Chem. Phys. Lett.* **2000**, *323*, 167. (b) Corbierre, M. K.; Lennox, R. B. *Chem. Mater.* **2005**, *17*, 5691.
- (9) Shields, S. P.; Richards, V. N.; Buhro, W. E. *Chem. Mater.* **2010**, *22*, 3212.
- (10) Pratsinis, S. E. *AIChE J.* **2010**, *56*, 3028.
- (11) Boissiere, C.; Grosso, D.; Chaumonnot, A.; Nicole, L.; Sanchez, C. *Adv. Mater.* **2011**, *23*, 599.
- (12) (a) Byeon, J. H.; Park, J. H.; Hwang, J. J. *Aerosol Sci.* **2008**, *39*, 888. (b) Byeon, J. H.; Kim, J.-W. *Thin Solid Films* **2010**, *519*, 700.
- (13) Byeon, J. H.; Roberts, J. T. *ACS Appl. Mater. Interfaces* **2012**, *4*, 2693.
- (14) (a) Thimsen, E. *Chem. Mater.* **2011**, *23*, 4612. (b) Huh, S. H.; Riu, D. H.; Naono, Y.; Taguchi, Y.; Kawabata, S.; Nakajima, A. *Appl. Phys. Lett.* **2007**, *91*, 093118. (c) Palgrave, R. G.; Parkin, I. P. *J. Am. Chem. Soc.* **2006**, *128*, 1587.
- (15) Byeon, J. H.; Kim, J.-W. *Atmos. Environ.* **2012**, *54*, 272.
- (16) To, D.; Dave, R.; Yin, X.; Sundaresan, S. *AIChE J.* **2009**, *55*, 2807.
- (17) (a) Henz, B. J.; Hawa, T.; Zachariah, M. R. *Langmuir* **2008**, *24*, 773. (b) Zhang, L.; Goddard, W. A., III; Jiang, S. J. *Chem. Phys.* **2002**, *117*, 7342. (c) Jang, S. S.; Jang, Y. H.; Kim, Y.-H.; Goddard, W. A., III; Flood, A. H.; Laursen, B. W.; Tseng, H.-R.; Stoddart, J. F.; Jeppesen, J. O.; Choi, J. W.; Steuerman, D. W.; Delonno, E.; Heath, J. R. *J. Am. Chem. Soc.* **2005**, *127*, 1563. (d) Mariscal, M. M.; Olmos-Asar, J. A.; Cutierrez-Wing, C.; Mayoral, A.; Yacaman, M. J. *Phys. Chem. Chem. Phys.* **2010**, *12*, 11785.
- (18) (a) Simard, J.; Briggs, C.; Boal, A. K.; Rotello, V. M. *Chem. Commun.* **2000**, *19*, 1943. (b) Shon, Y.-S.; Gross, S. M.; Dawson, B.; Porter, M.; Murray, R. W. *Langmuir* **2000**, *16*, 6555. (c) dell'Erba, I. E.; Hoppe, C. E.; Williams, R. J. J. *Langmuir* **2010**, *26*, 2042. (d) Yan, H.; Wong, C.; Chianese, A. R.; Luo, J.; Wang, L.; Yin, J.; Zhong, C.-J. *Chem. Mater.* **2010**, *22*, 5918.
- (19) (a) Jin, Y.; Wang, P.; Yin, D.; Liu, J.; Qin, L.; Yu, N.; Xie, G.; Li, B. *Colloids Surf., A* **2007**, *302*, 366. (b) Yee, C. K.; Jordan, R.; Ulman, A.; White, H.; King, A.; Rafailovich, M.; Sokolov, J. *Langmuir* **1999**, *15*, 3486. (c) Pham, T.; Jackson, J. B.; Halas, N. J.; Lee, T. R. *Langmuir* **2002**, *18*, 4915. (d) <http://www.science-and-fun.de/tools/>. (e) Ulman, A. *Chem. Rev.* **1996**, *96*, 1533.
- (20) Plant, D.; Tarbell, D. S.; Whiteman, C. J. *Am. Chem. Soc.* **1955**, *77*, 1572.
- (21) (a) Zhang, M.; Liu, M.; Xue, Y.-N.; Huang, S.-W.; Zhuo, R.-X. *Bioconjugate Chem.* **2009**, *20*, 440. (b) Wang, C.-H.; Chang, C.-W.; Peng, C.-A. *J. Nanopart. Res.* **2011**, *13*, 2749.